NANO LETTERS

pubs.acs.org/NanoLett Letter

# A Covalent Organic Framework for Fast-Charge and Durable Rechargeable Mg Storage

Ruimin Sun, Singyuk Hou, Chao Luo,* Xiao Ji, Luning Wang, Liqiang Mai,* and Chunsheng Wang*

Cite This: https://dx.doi.org/10.1021/acs.nanolett.0c01040 Read Online

ACCESS | Metrics & More | Article Recommendations | Supporting Information

**ABSTRACT:** High-safety, low-cost, and high-volumetric-capacity rechargeable magnesium batteries (RMBs) are promising alternatives to lithium ion batteries. However, lack of high-power, high-energy, and stable cathodes for RMBs hinders their commercialization. Herein, an environmentally benign, low-cost, and sustainable covalent organic framework (COF) cathode for Mg storage is reported for the first time. It delivers a high power density of 2.8 kW $kg^{-1}$, a high specific energy density of 146 Wh $kg^{-1}$, and an ultralong cycle life of 3000 cycles with a very slow capacity decay rate of 0.0196% per cycle, representing one of the best cathodes to date. The comprehensive electrochemical analysis proves that triazine ring sites in the COF are redox centers for reversible reaction with magnesium ions, and the ultrafast reaction kinetics are mainly attributed to pseudocapacitive behavior. The high-rate Mg storage of the COF offers new opportunities for the development of ultrastable and fast-charge RMBs.

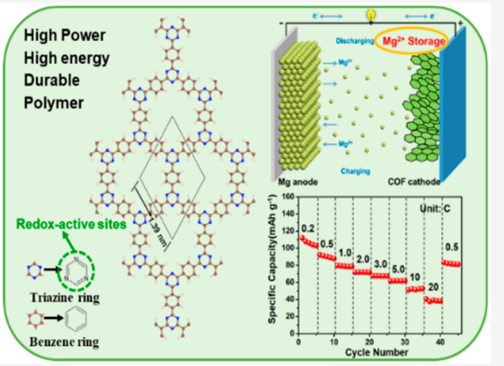


**KEYWORDS:** *Mg storage, cathode, porous covalent organic framework, fast charge, high energy density*



With the increasing demands of advanced energy storage devices for electric vehicles and smart grids, considerable research efforts have been devoted to developing safe, low-cost, and high-capacity rechargeable batteries.[1,2] Since the commercialization in 1991, lithium-ion batteries (LIBs) have dominated the energy storage market due to their high energy density and long cycle life.[3] However, safety concerns, limited lithium resources, and high cost hinder the ever-growing application of LIBs. Among battery systems beyond LIBs, rechargeable magnesium batteries (RMBs) are very promising for large scale energy storage, because magnesium (Mg) is not only abundant, inexpensive, and extremely safe under ambient atmosphere but also has nearly twice (3833 mAh $cm^{-3}$) the volumetric capacity of lithium (Li) anodes (2046 mAh $cm^{-3}$).[4−6] More importantly, different from Li and sodium (Na) anodes, Mg anodes are dendrite-free during long-term Mg plating and stripping, enabling RMBs to become inherently high-safety battery systems.[7] All of these merits make RMBs more promising in the market of low-cost and sustainable energy storage devices.

Despite these advantages, lack of high-performance cathode materials still impedes further development of RMBs. The intercalation chemistry of highly polarized $Mg^{2+}$ in cathode materials is complicated and sluggish, especially in inorganic cathodes, due to the strong electrostatic interaction between the divalent cations and host materials as well as the redistribution of electric charges of cations in the host lattices.[8] These cations exhibit several orders of magnitude higher diffusion barriers than $Li^+$ in the same cathode, compromising the electrochemical performance, or even preventing the intercalation of $Mg^{2+}$.[9] Furthermore, the most common electrolytes (chloride-containing electrolytes) in RMBs show narrow voltage windows and may generate irreversible passivation layers on anodes which prohibit the reversible Mg plating and stripping.[7,10,11] Up to now, Chevrel phase $Mo_6S_8$ is still the most promising inorganic cathode material for RMBs.[12] However, the low operating voltage, low capacity, and sluggish reaction kinetics preclude its commercial application. Therefore, searching for high-performance cathode materials is critical for the development of RMBs.

Compared to inorganic cathode materials, organic cathode materials are abundant, low-cost, sustainable, and environmentally benign. Moreover, most organic cathodes, with more flexible $Mg^{2+}$ transfer pathways and lower intermolecular forces than inorganic cathodes, are expected to improve reaction kinetics and cycling stability in RMBs.[13,14] However, most conventional organic compounds suffer from high solubility in organic electrolytes and low electronic conductivity, leading to fast capacity fading upon cycling.[15] Extensive efforts have been devoted to circumventing these two challenges. Liao and coworkers have synthesized 2,6-polyanthraquinone (26PAQ) and 1,4-polyanthraquinone (14PAQ) as cathodes, which exhibit

Received: March 9, 2020
Revised: April 5, 2020
Published: April 22, 2020




https://dx.doi.org/10.1021/acs.nanolett.0c01040
Nano Lett. XXXX, XXX, XXX−XXX

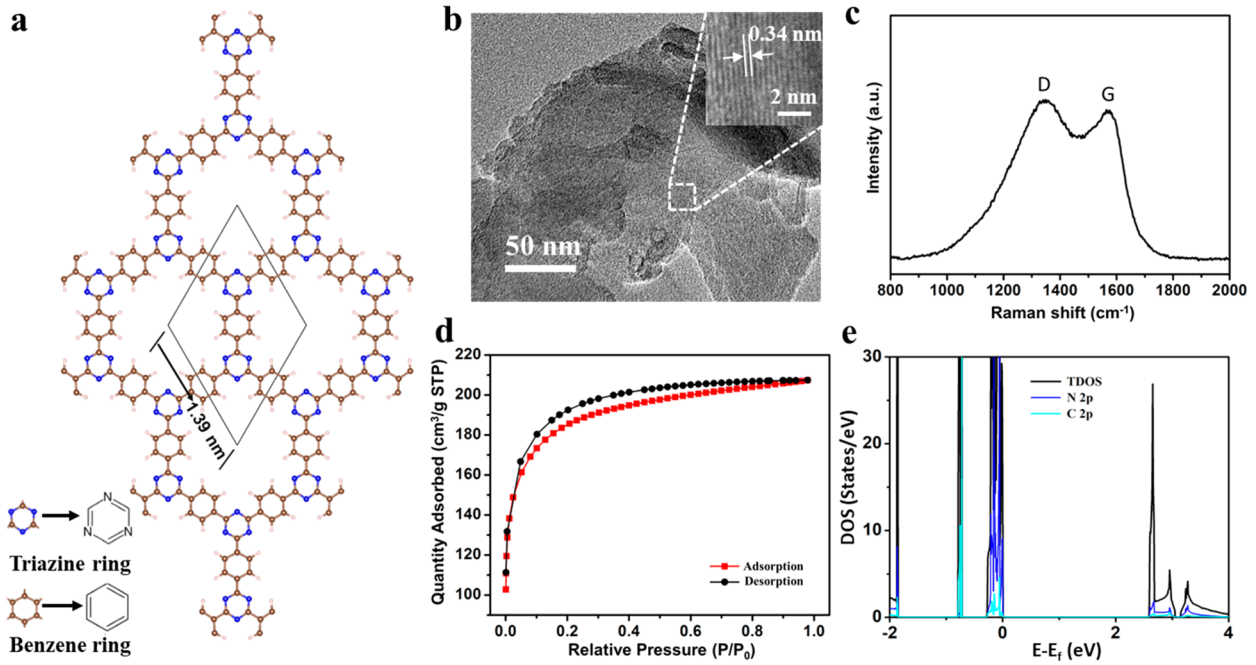


**Figure 1.** (a) Schematic illustration of the COF. (b) TEM images of the COF, showing a layered structure (the inset is HRTEM of the COF). (c) Raman spectrum and (d) nitrogen adsorption−desorption isotherms of the COF. (e) The total, C-2p orbital-resolved, and N-2p orbital-resolved DOS plots of the COF.

excellent battery performances in RMBs.[14] Mg-26PAQ can deliver over 100 mAh $g^{-1}$ discharge capacity at 0.5 C (130 mA $g^{-1}$) with 82% capacity retention after 100 cycles. For Mg-14PAQ, a discharge capacity of 104.9 mAh $g^{-1}$ can be retained at 0.5 C. Yao and co-workers also reported quinone-based polymer cathodes, poly(1,4-anthraquinone) (P14AQ), 2,5-dimethoxy-1,4-benzoquinone (DMBQ), and poly(P-(NDI2OD-T2)), in RMBs.[16] The specific energy of P14AQ was up to 243 Wh $kg^{-1}$, and the P(NDI2OD-T2) cells showed specific power up to 3.4 kW $kg^{-1}$ when tested in three-electrode cells. These organic materials deliver high energy densities that match or even exceed those Chevrel phase cathodes. More importantly, good structural tunability of organic electrode materials enables further performance optimization for RMBs.[17]

The covalent organic framework (COF) is a porous polymeric material composed of lightweight elements (C, H, N, and O) connected by covalent bonds.[18] It has received considerable research interests owing to its successful applications in catalysis,[19] gas storage,[20] energy storage,[21] etc. With cross-linked polymeric structure, the COF is stable and insoluble in organic electrolytes,[18] which is suitable for battery applications. In addition, its highly ordered porous structure and large surface area provide a sufficient electrode−electrolyte interface, leading to fast Mg ion diffusion and adequate accommodation for volume change during the electrochemical process. These advantages render COF materials promising cathode candidates for Mg storage.

Electrolytes also play a critical role in Mg storage.[22] Most electrolytes applied in RMBs are mainly based on the combination of a Mg-containing Lewis base (Grignard reagents and $MgCl_2$) and a Lewis acid ($AlCl_3$ and $AlPh_3$), known as Mg−chloride complex electrolytes.[22,23] However, the chloride-containing electrolytes are corrosive to noninert metal current collectors (stainless steel, aluminum) and have narrow voltage windows that inhibit the usability of high-voltage cathode materials.[6] Furthermore, in most chloride-containing electrolytes, $MgCl^+$ is the active cation that participates in the electrochemical reactions. Since the supply of chloride only comes from electrolytes, the specific energy of a battery is much lower than the $Mg^{2+}$ storage chemistry.[16] These disadvantages restrict the practical application of RMBs. Given these, it is imperative to search for desirable cathodes with high power and energy density and stable chloride-free electrolytes for Mg storage.

Herein, we report a high rate and stable COF cathode with a dendrite-free Mg anode and chloride-free as well as Mg-compatible electrolyte in Mg storage for the first time. This cathode material shows high power density (up to 2.8 kW $kg^{-1}$), high specific energy density (up to 146 Wh $kg^{-1}$), and long cycling stability, representing one of the best electrochemical performances among all reported organic cathodes to date. It delivers an initial discharge capacity of 102 mA h $g^{-1}$ at 0.5 C (1 C = 114 mA h $g^{-1}$) and still retains 70 and 52% of the capacity as the current density increases to 2 and 10 C, respectively. Moreover, at a high rate of 5 C, a reversible capacity of 72 mAh $g^{-1}$ can be achieved with a slow capacity decay rate of 0.0196% per cycle for 3000 cycles, representing one of the most outstanding cycling stabilities for organic Mg cathodes. The detailed kinetics analysis further explores the nature of charge storage. Rather than slow kinetics, large voltage hysteresis, and low reversibility for most RMBs, the COF-based cathode material demonstrates fast cation diffusion, ultrastable cycling stability, and ultrahigh rate properties owing to pseudocapacitive behavior with high capacitive contribution. Therefore, this type of porous COF cathode enables low cost, high sustainability, and high performance in Mg storage, which are demanded for most energy storage devices.

The COF was synthesized from rational polymerization of organic monomer 1,4-dicyanobenzene by heating it with $ZnCl_2$ in quartz ampules at 400 °C.[17,24,25] $ZnCl_2$ acts as a reaction


https://dx.doi.org/10.1021/acs.nanolett.0c01040
Nano Lett. XXXX, XXX, XXX−XXX

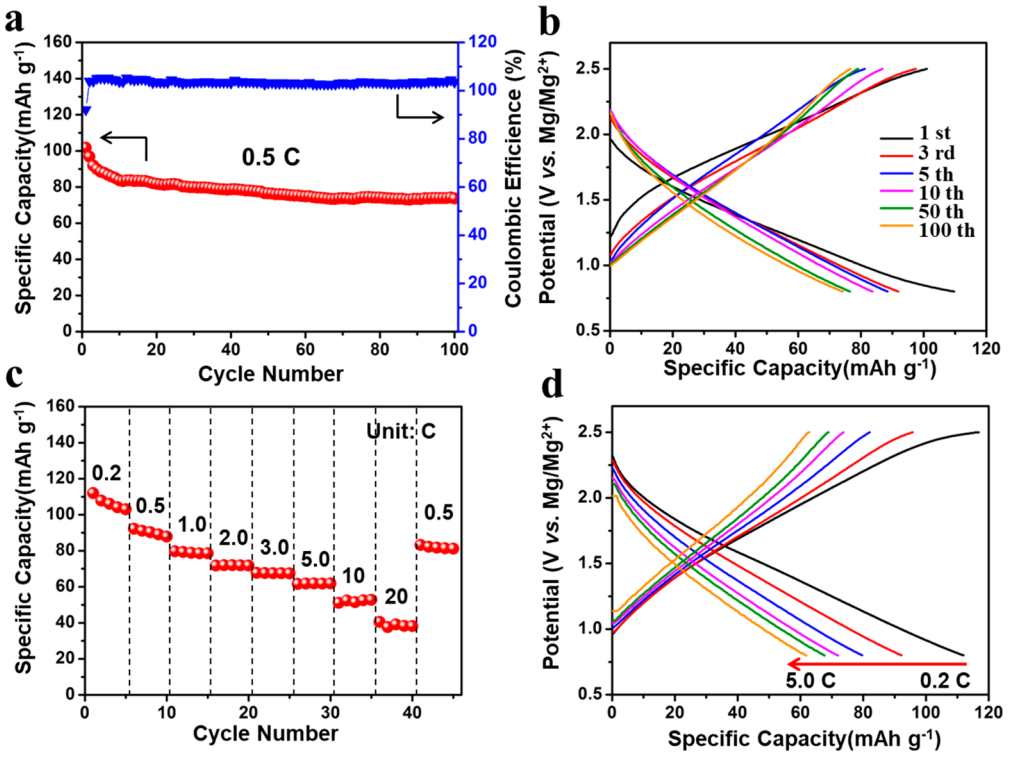


**Figure 2.** Electrochemical performance of the COF cathode in Mg storage. (a) Cyclic performance at 0.5 C (1 C = 114 mAh $g^{-1}$). (b) Discharge−charge curves of the COF at 0.5 C. (c) Rate performance. (d) Discharge−charge curves of electrodes at different rates.

catalyst for micropore formation. The COF material is a porous-honeycomb polymer composed of benzene rings and triazine rings with a two-dimensional (2D) layered structure.[24,26] First-principle computation based on density functional theory (DFT) was applied to calculate the optimized structures, showing a hexagonal micropore of 1.39 nm (Figure 1a). The morphology and detailed structure are observed by transmission electron microscopy (TEM) and high-resolution transmission electron microscopy (HRTEM) (Figure 1b). The COF material has a lamellar structure. The HRTEM image (inset of Figure 1b) from the edge of the sheet reveals that each sheet is an accumulation of (001) oriented sheets with an interlayer spacing around 3.4 Å. The phase of the COF was also identified by X-ray diffraction (XRD) (Figure S1), which shows a broad peak at 26.1°, corresponding to an interlayer distance of 3.4 Å for the aromatic sheets. The relatively broad peak suggests a short-range ordered framework, consisting of aromatic rings. The lamellar structure of the COF has a similar structure to boron oxide based covalent organic frameworks introduced by Yaghi et al.[27] The Raman spectrum in Figure 1c reveals the carbon hybridization in the COF. Typical peaks located at around 1330 and 1590 $cm^{-1}$ are attributed to the D and G bands of the COF, respectively. The G band is attributed to the vibration of $sp^2$ carbon atoms in the COF structure constituted by benzene rings and triazine rings, similar to porous graphite and graphene.[24,28] The D band is originated from defects and disorders in the 2D honeycomb layers. Fourier transform infrared (FT-IR) spectroscopy (Figure S2) further confirms the structure of the COF. The absorption band at 1507 $cm^{-1}$ represents the formation of triazine rings.[24,25] The Brunauer−Emmet−Teller (BET) surface area and pore size distribution were measured from nitrogen sorption isotherms (Figure 1d). The surface area of the COF is 428 $m^2$ $g^{-1}$ with a total pore volume of 0.18 $cm^3$ $g^{-1}$. The average pore size in the COF is 1.35 nm, which confirms the existence of micropores. In the X-ray photoelectron spectroscopy (XPS), the C 1s spectrum of the COF shows three distinct peaks located at 284.8, 286.8, and 288.2 eV, respectively (Figure S3). The peak at 284.8 eV is assigned to $sp^2$ carbons (—C—C—, —C═C—), the peak at 286.8 eV is attributed to N—C═N in triazine rings, while the peak at 288.2 eV is characteristic of those —C═O, suggesting an oxidized surface.[29,30] There are no signals of Zn 2p and Cl 2p for pristine COF material in XPS spectra (Figure S4). It confirms that $ZnCl_2$ catalyst is removed thoroughly and no chloride element remains in pristine COF material. The electronic properties of the COF were also investigated by DFT calculations. Figure 1e shows the total, C-2p orbital-resolved, and N-2p orbital-resolved density of state (DOS) plots of the COF material. The obvious overlap between the N-2p and C-2p orbitals suggests the strong intercalation between C and N atoms. The COF polymer exhibits a semiconductor character with a calculated band gap of 2.58 eV. The layer structured COF with reasonable electronic conductivity is a desirable cathode material for Mg storage.

The electrochemical performance of the COF cathode in Mg storage has been evaluated with 0.5 M $Mg(TFSI)_2$/DME-based electrolyte and Mg metal anode in coin cells. This DME-based electrolyte can achieve reversible Mg deposition and anodic stability at more than 4.0 V vs Mg (Figure S5). The electrochemical performance of bare Mg anodes in 0.5 M $Mg(TFSI)_2$/DME-based electrolyte was measured in a Mg//Mg symmetrical cell (Figure S6). The Mg//Mg cell exhibits a very stable voltage profile at a current density of 0.1 mA $cm^{-2}$. The cell overpotential is 78 mV throughout the whole 200 cycles, indicating the excellent stability of Mg plating/stripping in 0.5 M $Mg(TFSI)_2$/DME-based electrolyte. Dissolution of the COF in the 0.5 M $Mg(TFSI)_2$/DME-based electrolyte was


https://dx.doi.org/10.1021/acs.nanolett.0c01040
Nano Lett. XXXX, XXX, XXX−XXX

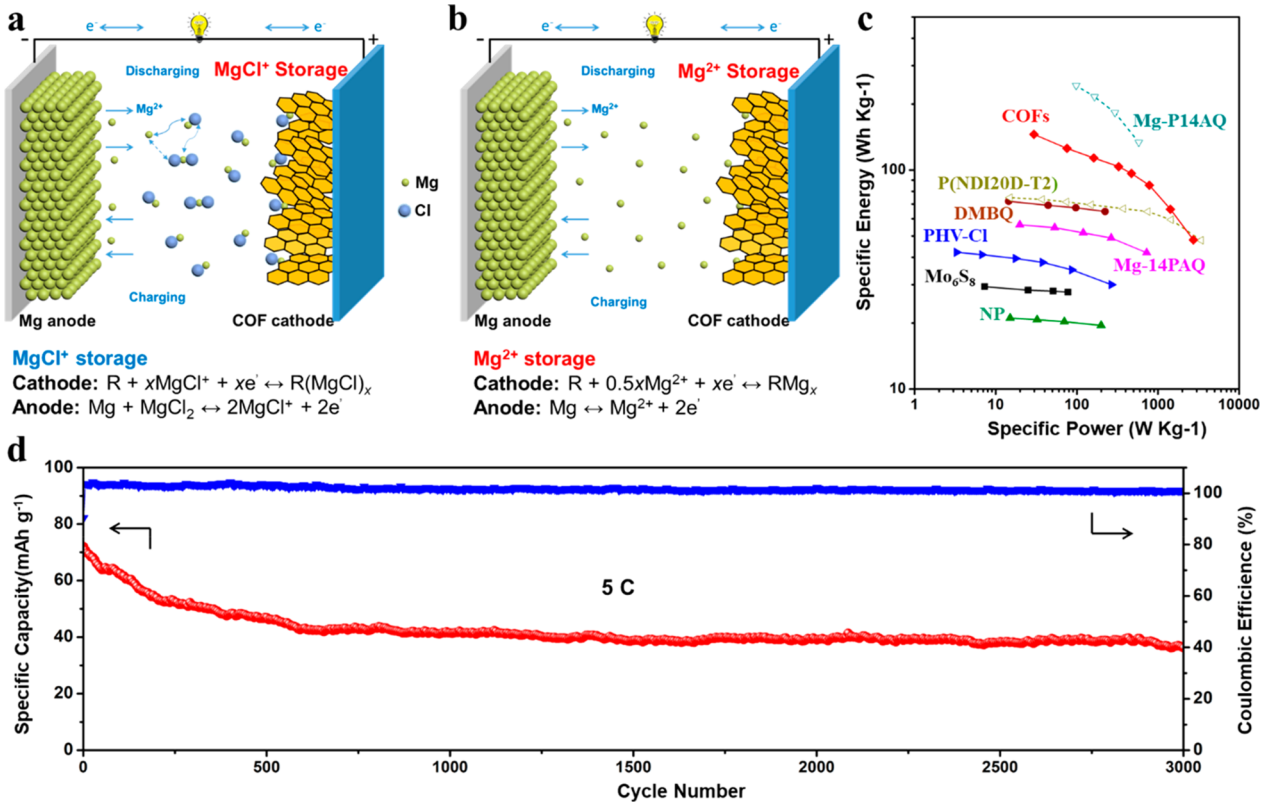


**Figure 3.** Schematic illustrations of the reaction mechanism and equations of organic cathodes in (a) chloride-containing and (b) chloride-free electrolytes. (c) Ragone plot of representative organic RMBs and Chevrel phase $Mo_6S_8$ considering the MgCl storage mechanism and the theoretically required amount of electrolytes (DMBQ,[15] Mg-14PAQ,[14] PHV-Cl,[31] naphthalene-hydrazine diimide polymer (NP),[13] P(NDI2OD-T2),[16] P14AQ,[16] and $Mo_6S_8$[32]). Solid line: energy densities were calculated from coin full cells. Dashed line: energy densities were taken from three-electrode cells by assuming cathodes can pair with Mg anodes. The values of discharge potentials obtained from three-electrode cells were used as discharge voltages by ignoring the stripping overpotential of Mg metal. Discharge capacities were also obtained from three-electrode cells. (d) Long-term cycling performance of the COF at 5 C.

performed (Figure S7). After a long time immersion of the COF in the electrolyte, the electrolyte solution still maintains transparent, indicating the insoluble nature of the COF in this electrolyte. The COF delivers an initial discharge capacity of 102 mAh $g^{-1}$ at 0.5 C (1 C = 114 mAh $g^{-1}$) (Figure 2a). During long-term cycling, the magnesiation/de-magnesiation process is highly reversible with a Coulombic efficiency of ~100%. The COF electrode shows sloping magnesiation/de-magnesiation curves from the 1st cycle to the 100th cycle at 0.5 C (Figure 2b). A reversible capacity of 74 mAh $g^{-1}$ can be retained after 100 cycles, demonstrating exceptional cycling stability. The rate performance of the COF was also measured at progressively increased current densities ranging from 0.2 to 20 C (Figure 2c,d). The specific capacity is 107 mAh $g^{-1}$ at 0.2 C, and it still retains 70 and 52% of the 0.2 C capacity as the current density increases to 2 and 10 C, respectively. The electrochemical performance of the COF was also tested in two chloride-containing electrolytes: 0.25 M $(PhMgCl)_2$/$AlCl_3$/THF (APC) and 0.25 M $Mg(TFSI)_2$/$MgCl_2$/DME (MTCC) electrolytes. As shown in Figure S8, the cycle stability and rate performance of the COF in these electrolytes are much worse than those in chloride-free $Mg(TFSI)_2$/DME-based electrolyte.

The ion storage chemistry plays a significant role in the specific energy of batteries. The electrochemical reaction comparison based on $MgCl^+$ and $Mg^{2+}$ storage chemistries in Mg batteries is shown in parts a and b of Figure 3, respectively. Energy density versus power density for organic cathodes in various reported Mg batteries are compared in Figure 3c. Since the most reported RMBs used chloride-containing Mg−chloride complex electrolytes, the salt involved in the magnesiation/de-magnesiation process should be counted. By counting salt mass in Mg batteries that use chloride-containing Mg−chloride complex electrolytes, COF/Mg full cells have the highest specific energy density among all of the reported Mg coin-cells, although some cathodes such as DMBQ,[15] P14AQ,[14] and poly(hexyl viologen dichloride) (PHV-Cl)[31] have a high specific energy density without counting salts in electrolytes (Figure S9).[16] However, since the salts in electrolytes participate in overall reactions in these cathodes, the specific energies of some materials are even lower than inorganic intercalation material ($Mo_6S_8$), considering the $MgCl^+$ storage mechanism.[16,32] The specific energy of our Mg storage COF material is not discounted (see the Supporting Information for detailed calculations), because of chloride-free electrolyte.[16] The detailed parameters based on Mg and MgCl storage chemistries are summarized in Tables S1 and S2, respectively. The specific energy and power densities of the COF reach up to 146 Wh $kg^{-1}$ and 2.8 kW $kg^{-1}$, respectively, standing out among those reported organic RMBs. Moreover, the cells also showed an ultralong cycle life. At a high rate of 5 C, an initial reversible capacity of 72 mAh $g^{-1}$ can be achieved with a very slow capacity decay rate of 0.0196% per cycle for 3000 cycles (Figure 3d), representing


https://dx.doi.org/10.1021/acs.nanolett.0c01040
Nano Lett. XXXX, XXX, XXX−XXX

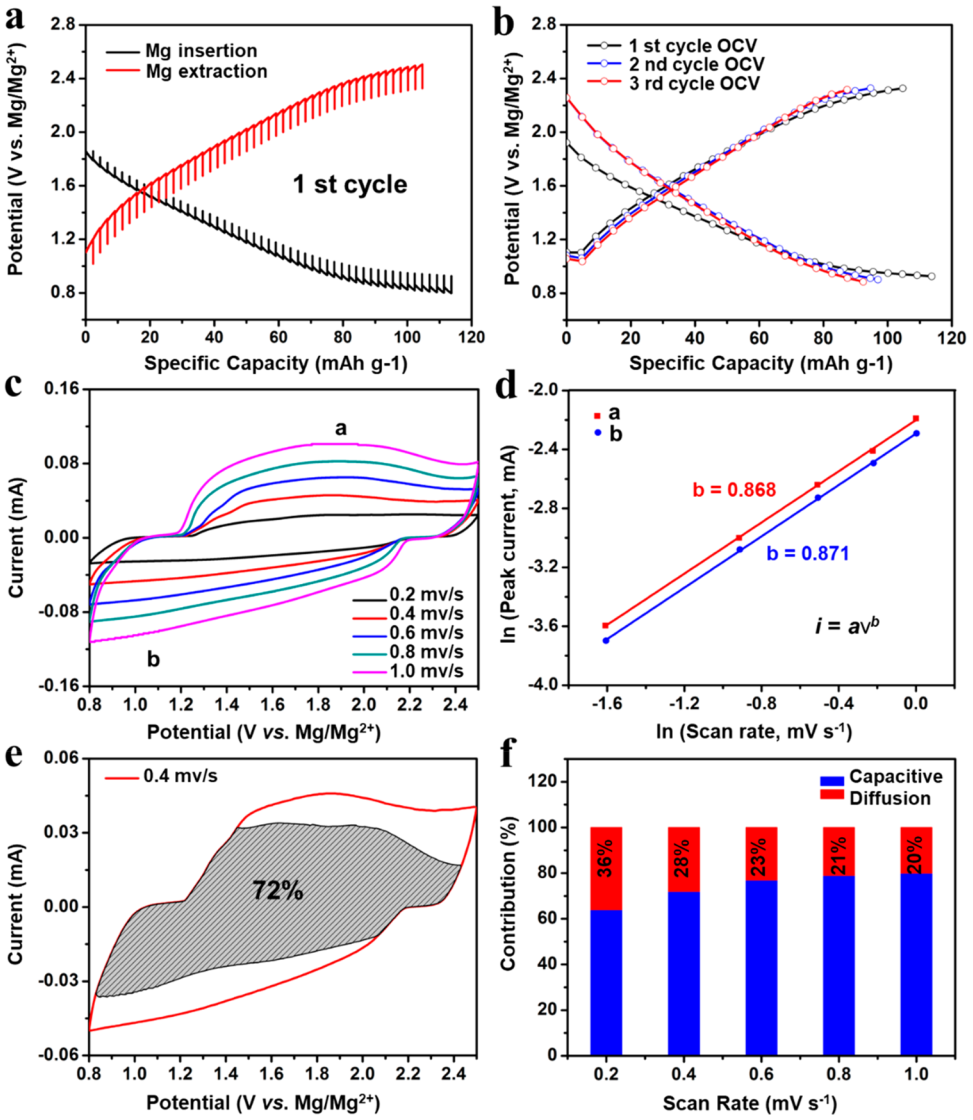


**Figure 4.** (a) Potential response of the COF electrode in the first cycle during GITT measurements. (b) Equilibrium potential versus specific capacity during GITT measurement (OCV: open circuit potential). (c) CV curves at different sweep rates. (d) The relationship of peak current and scan rate for the COF. (e) Capacitive contribution at 0.4 mV $s^{-1}$. (f) Capacity contributions at different scan rates.

one of the most outstanding long-term cycling stabilities for Mg batteries to date. The discharge−charge curve of the COF electrode after 3000 cycles is shown in Figure S10. Therefore, the excellent cyclability and high rate capability of the COF demonstrate that this porous polymer is a promising cathode material for high-performance Mg storage.

The quasi-equilibrium potential and polarization of the COF cathodes during charge/discharge process were further explored by the galvanostatic intermittent titration technique (GITT) and cyclic voltammetry (CV) scans at various scan rates. The COF delivered a reversible capacity of 114 mAh $g^{-1}$ according to the GITT result (Figure 4a). Figure 4b shows quasi-equilibrium potentials in the first three electrochemical cycles. No obvious discharge/charge plateaus can be observed, indicating that the battery does not undergo a phase transformation intercalation process.[33] The CV curves at different scan rates were recorded (Figure 4c). The CV currents ($i$) at different scan rates obey a power law relationship with scan rates ($\nu$): $i = a\nu^b$ ($a$ and $b$ are adjustable values).[34] The $b$-value, which can be determined by the slope of $\ln(\nu)-\ln(i)$ plots, is an indicator for reaction kinetics. For a redox reaction limited by diffusion, it is close to 0.5. While the $b$-value approaches 1, the reaction is mostly controlled by a capacitive process, which includes both pseudocapacitance and nonfaradaic double layer contribution.[18] Figure 4d shows the $b$-value at different oxidation and reduction states. Since $b$-values (0.868 and 0.871) approach 1, the battery is mainly controlled by a capacitive process.

To further quantify the capacitive and diffusion-controlled contributions to the whole capacity, the total current response ($i$) at fixed potential ($V$) can be separated into two mechanisms of capacitive ($k_1\nu$) and diffusion-controlled processes ($k_2\nu^{1/2}$), according to the following equation:[35,36]

$$i = k_1\nu + k_2\nu^{1/2} \quad (1)$$

By determining both $k_1$ and $k_2$ constants, the fractions of current from the capacitive contribution and diffusion are distinguished. 72% of the total charge comes from the capacitive contribution at a scan rate of 0.4 mV $s^{-1}$ (Figure 4e), which contributes to the high rate and stable long-term


https://dx.doi.org/10.1021/acs.nanolett.0c01040
Nano Lett. XXXX, XXX, XXX−XXX

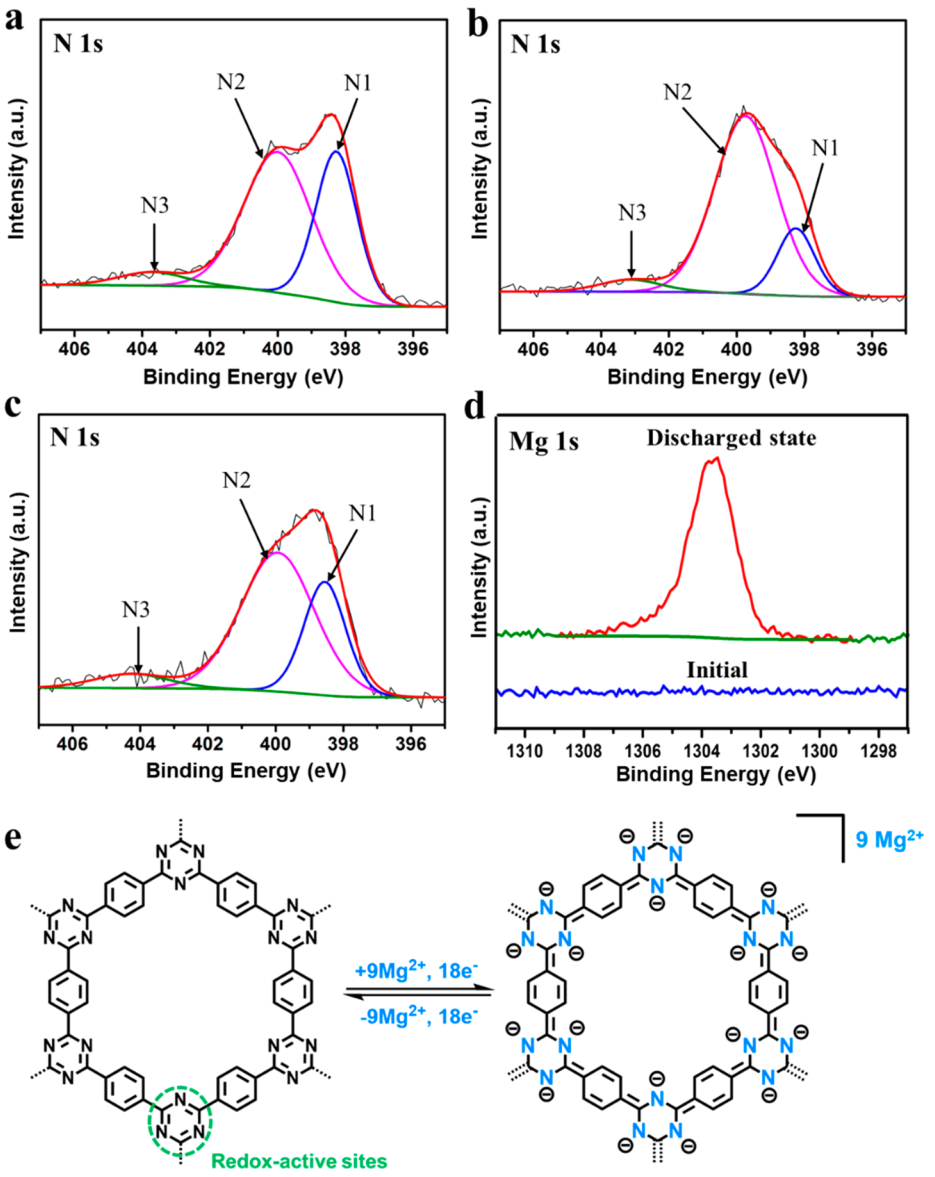


**Figure 5.** XPS spectra of the COF collected at different electrochemical states. N 1s spectra at (a) original state, (b) discharged state, and (c) charged state. (d) The respective *ex situ* Mg 1s XPS spectra of the COF at denoted states. (e) Chemical structure and possible electrochemical redox mechanism of the COF.

cycling performance. Figure 4f shows capacity contributions of the COF at different scan rates. The capacitive contribution increases with increased scan rates.

The amorphous and stable structure of the COF networks with interconnected electrolyte-filled pores provides more active sites for fast $Mg^{2+}$ diffusion and short magnesium ion transfer pathways, minimizing the sluggish solid-state ion transport effect. During the ion and electron transfer process, active cations can easily enter the open spaces in polymers. All of these are a prerequisite for pseudocapacitance, thus leading to fast reaction kinetics, ultrastable cycle life, and high power and energy densities.[36−38] In contrast to inorganic materials with crystalline structures, which usually display slow solid-state ion diffusion and phase transformation,[39] the soft and porous COF enables fast-charge capability, while maintaining long cyclic stability. These offer an opportunity to enhance electrochemical properties and reaction kinetics, revolutionizing conventional low-power and poor-cycle-life multivalent-ion battery chemistries.

XPS was performed to investigate surface bonding and chemical composition changes of the COF cathode during the charge storage process. The energy storage mechanism is investigated through tracking variations of N 1s and Mg 1s peaks during the discharge/charge process. The C 1s peak at 284.8 eV in pristine COF is used as a reference binding energy. The N 1s spectrum of the fresh COF electrode (Figure 5a) shows three peaks centered at 398.1, 400, and 401 eV, corresponding to pyridinic-N (N1) in triazine rings, pyrrolic-N (N2), and graphitic-N (N3), respectively.[40] N1 and N2 represent nitrogen atoms, bonding to two carbon atoms, and donate one or two p-electrons to the aromatic $\pi$-system. N3 is attributed to quaternary or protonated nitrogen.[41] When the COF electrode is at a discharged (magnesiation) state (Figure 5b), the intensity of the N1 peak decreases remarkably, due to the interaction between $Mg^{2+}$ and —C═N— in triazine rings.[42−44] The N1 peak is recovered when the electrode is at a charged (de-magnesiation) state, suggesting the reversible magnesiation and de-magnesiation of —C═N— in triazine


https://dx.doi.org/10.1021/acs.nanolett.0c01040
Nano Lett. XXXX, XXX, XXX−XXX

rings (Figure 5c). Therefore, —C═N— sites in triazine rings are redox-active centers of the COF. Figure 5d shows the Mg 1s core level spectra of the COF in pristine and discharged states. No signal for magnesium can be detected in the XPS spectrum of fresh COF. When discharged to 0.8 V, an obvious Mg 1s peak can be observed, indicating the redox reaction between $Mg^{2+}$ and the COF. As triazine rings are redox sites for porous COF electrodes, each COF repetitive unit can reversibly bond with a maximum number of nine Mg ions during the charge/discharge process, as shown in Figure 5e. Thus, this COF-based cathode material is promising for developing high-energy and high-power magnesium storage devices.

The plenty of electrochemically active nitrogen groups in the COF, especially N-1 and N-3, are important for enhancing the capacitive process.[41,45] N-1 provides numerous active sites for electrical double-layer capacitance and pseudocapacitance. N-3 improves conductivity, which benefits electron transport.[45] As a result, the N-containing and porous structure of the COF cathode can effectively improve the electrochemical performance for $Mg^{2+}$ storage.[18,33]

Based on the above results, we defined a triazine ring with a benzene ring ($C_9N_3$) as the unit cell of the COF electrode. The overall electrochemical reaction of COF-based RMBs can be described as follows:

anode:

$$Mg \leftrightarrow Mg^{2+} + 2e^{-}$$

cathode:

$$C_9N_3 + xMg^{2+} + 2xe^{-} \leftrightarrow [(Mg^{2+})_x(C_9N_3)^{-2x}]$$

In summary, a triazine-based porous COF is applied as a cathode material in RMBs. It delivers a specific power density of 2.8 kW $kg^{-1}$ and a high specific energy density of 146 Wh $kg^{-1}$. The COF cathode shows a discharge capacity of 107 mA h $g^{-1}$ at 0.2 C. A reversible capacity of 72 mAh $g^{-1}$ can be achieved at a high rate of 5 C with a slow capacity decay rate of 0.0196% per cycle for 3000 cycles, representing one of the most outstanding long-term cycling stabilities for Mg batteries to date. The detailed characterizations and electrochemical kinetic analysis reveal that the charge storage is controlled by a capacitive process, ensuring fast reaction kinetics, ultrastable cycle life, high power, and energy densities. *Ex situ* XPS results demonstrate that redox-active sites are based on triazine rings in the COF. Our findings offer a new direction for developing environmentally benign, fast-charge, and ultrastable RMB cathode materials, which also resolve the cost concern and sluggish $Mg^{2+}$ storage kinetics of inorganic crystalline cathode materials.

## ■ ASSOCIATED CONTENT

### Supporting Information

The Supporting Information is available free of charge at https://pubs.acs.org/doi/10.1021/acs.nanolett.0c01040.

Experimental details; XRD, FTIR, and XPS characterizations of obtained material; CV curve of $Mg(TFSI)_2$/DME-based electrolyte; Ragone plot of organic Mg batteries without considering the theoretically required amount of electrolytes; GITT curves of the COF electrode in the second and third cycles (PDF)

## ■ AUTHOR INFORMATION


### Corresponding Authors

**Chao Luo** − *Department of Chemistry and Biochemistry, George Mason University, Fairfax, Virginia 22030, United States;* orcid.org/0000-0001-8497-8548; Email: cluo@gmu.edu

**Liqiang Mai** − *State Key Laboratory of Advanced Technology for Materials Synthesis and Processing, Wuhan University of Technology, Wuhan 430070, China;* orcid.org/0000-0003-4259-7725; Email: mlq518@whut.edu.cn

**Chunsheng Wang** − *Department of Chemical and Biomolecular Engineering, University of Maryland, College Park, Maryland 20742, United States;* orcid.org/0000-0002-8626-6381; Email: cswang@umd.edu

### Authors

**Ruimin Sun** − *Department of Chemical and Biomolecular Engineering, University of Maryland, College Park, Maryland 20742, United States; State Key Laboratory of Advanced Technology for Materials Synthesis and Processing, Wuhan University of Technology, Wuhan 430070, China*

**Singyuk Hou** − *Department of Chemical and Biomolecular Engineering, University of Maryland, College Park, Maryland 20742, United States*

**Xiao Ji** − *Department of Chemical and Biomolecular Engineering, University of Maryland, College Park, Maryland 20742, United States*

**Luning Wang** − *Department of Chemical and Biomolecular Engineering, University of Maryland, College Park, Maryland 20742, United States;* orcid.org/0000-0002-3785-1787

Complete contact information is available at: https://pubs.acs.org/10.1021/acs.nanolett.0c01040


### Author Contributions

R.S., L.M., and C.W. conceived the idea. R.S., S.H., and L.W. carried out the synthesis and electrochemical evaluation. X.J. performed DFT calculations. R.S., S.H., and C.L. helped with material characterization and manuscript preparation. All authors discussed the results and commented on the manuscript.

### Notes

The authors declare no competing financial interest.

## ■ ACKNOWLEDGMENTS

We thank Dr. Karen J. Gaskell at the Surface Analysis Center of University of Maryland for the help on the XPS test and data analysis. This project was supported by the Department of Energy (DOE) Office of Energy Efficiency and Renewable Energy (EERE) through Battery500 Consortium under contract No. DE-EE0008202. C.L. acknowledges the support of the George Mason University, College of Science Postdoctoral Fellowship, under Award No. 183904. R.S. acknowledges the support of the China Postdoctotal Science Foundation (2018M642938, 2019T120691) and Fundamental Research Funds for the Central Universities (3120619324).

## ■ REFERENCES

(1) Larcher, D.; Tarascon, J. M. Towards greener and more sustainable batteries for electrical energy storage. *Nat. Chem.* **2015**, *7*, 19.

(2) Parker, J. F.; Chervin, C. N.; Pala, I. R.; Machler, M.; Burz, M. F.; Long, J. W.; Rolison, D. R. Rechargeable nickel-3D zinc batteries: an energy-dense, safer alternative to lithium-ion. *Science* **2017**, *356*, 415−418.

(3) Yoshino, A. The birth of the lithium-ion battery. *Angew. Chem., Int. Ed.* **2012**, *51*, 5798−5800.
(4) Esparcia, E. A., Jr; Chae, M. S.; Ocon, J. D.; Hong, S.-T. Ammonium vanadium bronze ($NH_4V_4O_{10}$) as a high-capacity cathode material for nonaqueous magnesium-ion batteries. *Chem. Mater.* **2018**, *30*, 3690−3696.
(5) Xu, M.; Lei, S.; Qi, J.; Dou, Q.; Liu, L.; Lu, Y.; Huang, Q.; Shi, S.; Yan, X. Opening magnesium storage capability of two-dimensional Mxene by intercalation of cationic surfactant. *ACS Nano* **2018**, *12*, 3733−3740.
(6) Sun, R.; Pei, C.; Sheng, J.; Wang, D.; Wu, L.; Liu, S.; An, Q.; Mai, L. High-rate and long-life $VS_2$ cathodes for hybrid magnesium-based battery. *Energy Storage Mater.* **2018**, *12*, 61−68.
(7) Muldoon, J.; Bucur, C. B.; Gregory, T. Fervent hype behind magnesium batteries: an open call to synthetic chemists-electrolytes and cathodes needed. *Angew. Chem., Int. Ed.* **2017**, *56*, 12064−12084.
(8) McAllister, B. T.; Kyne, L. T.; Schon, T. B.; Seferos, D. S. Potential for disruption with organic magnesium-ion batteries. *Joule* **2019**, *3*, 620−624.
(9) Attias, R.; Salama, M.; Hirsch, B.; Gofer, Y.; Aurbach, D. Solvent effects on the reversible intercalation of magnesium-ions into $V_2O_5$ electrodes. *ChemElectroChem* **2018**, *5*, 3514−3524.
(10) Canepa, P.; Sai Gautam, G.; Hannah, D. C.; Malik, R.; Liu, M.; Gallagher, K. G.; Persson, K. A.; Ceder, G. Odyssey of multivalent cathode materials: open questions and future challenges. *Chem. Rev.* **2017**, *117*, 4287−4341.
(11) Kong, L.; Yan, C.; Huang, J. Q.; Zhao, M. Q.; Titirici, M. M.; Xiang, R.; Zhang, Q. A review of advanced energy materials for magnesium-sulfur batteries. *Energy Environ. Mater.* **2018**, *1*, 100−112.
(12) Fan, X.; Wang, F.; Ji, X.; Wang, R.; Gao, T.; Hou, S.; Chen, J.; Deng, T.; Li, X.; Chen, L. A universal organic cathode for ultrafast lithium and multivalent metal batteries. *Angew. Chem., Int. Ed.* **2018**, *57*, 7146−7150.
(13) Bančič, T.; Bitenc, J.; Pirnat, K.; Lautar, A. K.; Grdadolnik, J.; Vitanova, A. R.; Dominko, R. Electrochemical performance and redox mechanism of naphthalene-hydrazine diimide polymer as a cathode in magnesium battery. *J. Power Sources* **2018**, *395*, 25−30.
(14) Pan, B.; Huang, J.; Feng, Z.; Zeng, L.; He, M.; Zhang, L.; Vaughey, J. T.; Bedzyk, M. J.; Fenter, P.; Zhang, Z.; Burrell, A. K.; Liao, C. Polyanthraquinone-based organic cathode for high-performance rechargeable magnesium-ion batteries. *Adv. Energy Mater.* **2016**, *6*, 1600140.
(15) Pan, B.; Zhou, D.; Huang, J.; Zhang, L.; Burrell, A. K.; Vaughey, J. T.; Zhang, Z.; Liao, C. 2,5-Dimethoxy-1,4-Benzoquinone (DMBQ) as organic cathode for rechargeable magnesium-ion batteries. *J. Electrochem. Soc.* **2016**, *163*, A580−A583.
(16) Dong, H.; Liang, Y.; Tutusaus, O.; Mohtadi, R.; Zhang, Y.; Hao, F.; Yao, Y. Directing Mg-Storage chemistry in organic polymers toward high-energy Mg batteries. *Joule* **2019**, *3*, 782−793.
(17) Sakaushi, K.; Nickerl, G.; Wisser, F. M.; Nishio-Hamane, D.; Hosono, E.; Zhou, H.; Kaskel, S.; Eckert, J. An energy storage principle using bipolar porous polymeric frameworks. *Angew. Chem., Int. Ed.* **2012**, *51*, 7850−7854.
(18) Zhang, X.; Zhu, G.; Wang, M.; Li, J.; Lu, T.; Pan, L. Covalent-organic-frameworks derived N-doped porous carbon materials as anode for superior long-life cycling lithium and sodium ion batteries. *Carbon* **2017**, *116*, 686−694.
(19) Jiang, X.; Wang, P.; Zhao, J. 2D covalent triazine framework: a new class of organic photocatalyst for water splitting. *J. Mater. Chem. A* **2015**, *3*, 7750−7758.
(20) Lee, Y. J.; Talapaneni, S. N.; Coskun, A. Chemically activated covalent triazine frameworks with enhanced textural properties for high capacity gas storage. *ACS Appl. Mater. Interfaces* **2017**, *9*, 30679−30685.
(21) Li, Y.; Zheng, S.; Liu, X.; Li, P.; Sun, L.; Yang, R.; Wang, S.; Wu, Z. S.; Bao, X.; Deng, W. Q. Conductive microporous covalent triazine-based framework for high-performance electrochemical capacitive energy storage. *Angew. Chem., Int. Ed.* **2018**, *57*, 7992−7996.
(22) Luo, J.; Bi, Y.; Zhang, L.; Zhang, X.; Liu, T. L. A stable, non-corrosive perfluorinated pinacolatoborate mg electrolyte for rechargeable Mg batteries. *Angew. Chem., Int. Ed.* **2019**, *58*, 6967−6971.
(23) Deivanayagam, R.; Ingram, B. J.; Shahbazian-Yassar, R. Progress in development of electrolytes for magnesium batteries. *Energy Storage Mater.* **2019**, *21*, 136−153.
(24) Sakaushi, K.; Hosono, E.; Nickerl, G.; Gemming, T.; Zhou, H.; Kaskel, S.; Eckert, J. Aromatic porous-honeycomb electrodes for a sodium-organic energy storage device. *Nat. Commun.* **2013**, *4*, 1485.
(25) Kuhn, P.; Antonietti, M.; Thomas, A. Porous, covalent triazine-based frameworks prepared by ionothermal synthesis. *Angew. Chem., Int. Ed.* **2008**, *47*, 3450−3453.
(26) Yu, S. Y.; Mahmood, J.; Noh, H. J.; Seo, J. M.; Jung, S. M.; Shin, S. H.; Im, Y. K.; Jeon, I. Y.; Baek, J. B. Direct synthesis of a covalent triazine-based framework from aromatic amides. *Angew. Chem., Int. Ed.* **2018**, *57*, 8438−8442.
(27) Cote, A. P.; Benin, A. I.; Ockwig, N. W.; O'Keeffe, M.; Matzger, A. J.; Yaghi, O. M. Porous, crystalline, covalent organic frameworks. *Science* **2005**, *310*, 1166−1170.
(28) Sun, R.; Wei, Q.; Li, Q.; Luo, W.; An, Q.; Sheng, J.; Wang, D.; Chen, W.; Mai, L. Vanadium sulfide on reduced graphene oxide layer as a promising anode for sodium ion battery. *ACS Appl. Mater. Interfaces* **2015**, *7*, 20902−20908.
(29) Jiang, Y.; Oh, I.; Joo, S. H.; Buyukcakir, O.; Chen, X.; Lee, S. H.; Huang, M.; Seong, W. K.; Kim, J. H.; Rohde, J.-U. Organic radical-linked covalent triazine framework with paramagnetic behavior. *ACS Nano* **2019**, *13*, 5251−5258.
(30) Hellgren, N.; Haasch, R. T.; Schmidt, S.; Hultman, L.; Petrov, I. Interpretation of X-ray photoelectron spectra of carbon-nitride thin films: new insights from in situ XPS. *Carbon* **2016**, *108*, 242−252.
(31) Ikhe, A. B.; Naveen, N.; Sohn, K.-S.; Pyo, M. Polyviologen as a high energy density cathode in magnesium-ion batteries. *Electrochim. Acta* **2018**, *283*, 393−400.
(32) Saha, P.; Jampani, P. H.; Datta, M. K.; Okoli, C. U.; Manivannan, A.; Kumta, P. N. A convenient approach to $Mo_6S_8$ chevrel phase cathode for rechargeable magnesium battery. *J. Electrochem. Soc.* **2014**, *161*, A593−A598.
(33) Li, S.; Qiu, J.; Lai, C.; Ling, M.; Zhao, H.; Zhang, S. Surface capacitive contributions: towards high rate anode materials for sodium ion batteries. *Nano Energy* **2015**, *12*, 224−230.
(34) Luo, C.; Xu, G. L.; Ji, X.; Hou, S.; Chen, L.; Wang, F.; Jiang, J.; Chen, Z.; Ren, Y.; Amine, K. Reversible redox chemistry of azo compounds for sodium-ion batteries. *Angew. Chem., Int. Ed.* **2018**, *57*, 2879−2883.
(35) Cook, J. B.; Kim, H. S.; Yan, Y.; Ko, J. S.; Robbennolt, S.; Dunn, B.; Tolbert, S. H. Mesoporous $MoS_2$ as a transition metal dichalcogenide exhibiting pseudocapacitive Li and Na-ion charge storage. *Adv. Energy Mater.* **2016**, *6*, 1501937.
(36) Kim, H.-S.; Cook, J. B.; Lin, H.; Ko, J. S.; Tolbert, S. H.; Ozolins, V.; Dunn, B. Oxygen vacancies enhance pseudocapacitive charge storage properties of $MoO_{3-x}$. *Nat. Mater.* **2017**, *16*, 454.
(37) Sun, R.; Wei, Q.; Sheng, J.; Shi, C.; An, Q.; Liu, S.; Mai, L. Novel layer-by-layer stacked $VS_2$ nanosheets with intercalation pseudocapacitance for high-rate sodium ion charge storage. *Nano Energy* **2017**, *35*, 396−404.
(38) Sun, R.; Liu, S.; Wei, Q.; Sheng, J.; Zhu, S.; An, Q.; Mai, L. Mesoporous $NiS_2$ nanospheres anode with pseudocapacitance for high-rate and long-life sodium-ion battery. *Small* **2017**, *13*, 1701744.
(39) Han, F.; Westover, A. S.; Yue, J.; Fan, X.; Wang, F.; Chi, M.; Leonard, D. N.; Dudney, N. J.; Wang, H.; Wang, C. High electronic conductivity as the origin of lithium dendrite formation within solid electrolytes. *Nat. Energy* **2019**, *4*, 187.
(40) Osadchii, D. Y.; Olivos-Suarez, A. I.; Bavykina, A. V.; Gascon, J. Revisiting nitrogen species in covalent triazine frameworks. *Langmuir* **2017**, *33*, 14278−14285.
(41) Wu, J.; Zhang, D.; Wang, Y.; Hou, B. Electrocatalytic activity of nitrogen-doped graphene synthesized via a one-pot hydrothermal process towards oxygen reduction reaction. *J. Power Sources* **2013**, *227*, 185−190.


https://dx.doi.org/10.1021/acs.nanolett.0c01040
Nano Lett. XXXX, XXX, XXX−XXX

(42) Mao, M.; Luo, C.; Pollard, T. P.; Hou, S.; Gao, T.; Fan, X.; Cui, C.; Yue, J.; Tong, Y.; Yang, G.; Deng, T.; Zhang, M.; Ma, J.; Suo, L.; Borodin, O.; Wang, C. A pyrazine-based polymer for fast-charge batteries. *Angew. Chem., Int. Ed.* **2019**, *58*, 17820−17826.
(43) Xie, P.; Rong, M. Z.; Zhang, M. Q. Moisture battery formed by direct contact of magnesium with foamed polyaniline. *Angew. Chem., Int. Ed.* **2016**, *55*, 1805−1809.
(44) Rajagopalan, R.; Iroh, J. O. Characterization of polyaniline-polypyrrole composite coatings on low carbon steel: a XPS and infrared spectroscopy study. *Appl. Surf. Sci.* **2003**, *218*, 58−69.
(45) Sun, L.; Tian, C.; Fu, Y.; Yang, Y.; Yin, J.; Wang, L.; Fu, H. Nitrogen-doped porous graphitic carbon as an excellent electrode material for advanced supercapacitors. *Chem. - Eur. J.* **2014**, *20*, 564−574.


https://dx.doi.org/10.1021/acs.nanolett.0c01040
*Nano Lett.* XXXX, XXX, XXX−XXX